

Singularity Avoidance as Manipulability Maximization Using Continuous Time Gaussian Processes

Filip Marić^{*†}, Oliver Limoyo^{*}, Luka Petrović[†], Ivan Petrović[†], Jonathan Kelly^{*}

Abstract—A significant challenge in motion planning is to avoid being in or near *singular configurations*, that is, configurations in joint space that result in the loss of the ability to move in certain directions in task space. A robotic system’s manipulability is reduced even in regions that are in close proximity to (i.e., neighbouring) a singularity. In this work we examine singularity avoidance in a motion planning context, that is, finding a trajectory which minimizes proximity to singular regions, subject to constraints. Representing the trajectory as a sample taken from a continuous time Gaussian process, we define a likelihood associated with singularity avoidance. We leverage recent work on motion planning using exactly sparse Gaussian processes and a factor graph representation to maximize the singularity avoidance likelihood using a *maximum a posteriori* (MAP) estimator. Viewing the MAP problem as inference on a factor graph, we use gradient information from interpolated states to maximize the trajectory’s overall manipulability. Both qualitative and quantitative analysis of experimental data show increases in manipulability which results in smooth trajectories with visibly more dexterous configurations.

I. INTRODUCTION

Motion planning is a fundamental challenge for robotic systems executing complex tasks. Rapid and successful planning, and replanning in response to state or environment changes, is expected when real-time trajectory optimization methods are employed. Given a set of constraints and an objective, it is possible for such methods to produce a trajectory requiring large joint space velocities in order to achieve small task space changes. The goal of singularity avoidance (see below) in motion planning is to generate trajectories avoiding such configurations. The arm trajectory shown on the left side of Fig. 1 is an example in which the configuration is initially (and throughout the motion) nearly singular, with the arm fully extended. On the right side of Fig. 1 is a trajectory that results in the same 3D position in task space of the end effector, but that avoids these near-singular configurations.

Trajectory optimization methods often rely on the robot’s the Jacobian matrix [1]–[3]. Configurations which result in the Jacobian matrix being ill-conditioned or rank-deficient are known as singular states or *singularities*. Singularities are not desirable in trajectory optimization problems as they

This research has been partly supported by the European Regional Development Fund under the grant KK.01.1.1.01.0009 (DATACROSS).

^{*} Filip Marić, Oliver Limoyo and Jonathan Kelly are with the University of Toronto, Institute for Aerospace Studies, Space and Terrestrial Autonomous Robotic Systems laboratory, Canada. {<first name>.<last name>@robotics.utoronto.ca}

[†] Filip Marić, Luka Petrović and Ivan Petrović are with the University of Zagreb, Faculty of Electrical Engineering and Computing, Laboratory for Autonomous Systems and Mobile Robotics, Croatia. {<first name>.<last name>@fer.hr}



Fig. 1: Comparison of two solutions for reaching a 3D point (position) goal from a given near-singular starting configuration (caused by fully extending the arm). The left image shows a purely inverse kinematic approach, which maintains low manipulability throughout. The image on the right shows a trajectory generated by our method, which attempts to avoid excessive arm extension.

result in the loss of one or more degrees of freedom, immobilizing the system in certain task space directions. Moreover, it is undesirable for configurations to neighbour a singularity, as high joint velocities translate to small task space changes in these regions. It is also worth noting that singularities often coincide with configurations that have undesirable dynamic properties (e.g., a fully extended manipulator). Avoiding singularities is also beneficial in situations where frequent replanning is required, since an initial trajectory might be replanned into a singular configuration due to a constraint such as obstacle avoidance.

In this paper we propose a novel method that considers singularity avoidance as a probabilistic inference problem, where we define the likelihood of a configuration *not* being singular using a well known manipulability measure [4]. By viewing the trajectory as a sample from a continuous time Gaussian process [5], a maximum a posteriori (MAP) estimator can be used to find a solution that is, locally, in minimum proximity to a singular region [6]. By formulating this problem as inference on a factor graph [7], one can use the information provided by the continuous-time representation to achieve very substantial improvements in certain cases. Additionally, replanning on a factor graph can be performed in a very efficient manner using the Smoothing and Mapping (SAM) family of algorithms [8]. We make the following contributions herein:

- (i) we define the likelihood of a given configuration not being singular using a manipulability measure,
- (ii) we achieve singularity avoidance by maximizing the associated likelihood over a continuous trajectory using a MAP estimator, and

- (iii) we demonstrate that the likelihood gradient information from interpolated states can be used to achieve further improvements in certain cases.

II. RELATED WORK

A configuration's proximity to a singularity can be inferred using the manipulability ellipsoid, which gives a measure of the robots capacity to perform task space motions. The manipulability measure introduced by Yoshikawa [4] is proportional to this ellipsoid's volume and has previously been used for singularity avoidance in motion planning. Velocity-level redundancy resolution [9], search [10], and optimization [11] methods have been used to maximize the manipulability measure with the goal of singularity avoidance. Conceptually our method is closest to [11], where an inverse kinematics problem is formulated as a quadratic program (QP) and manipulability is maximized by adding it to the objective function while maintaining Cartesian constraints. Our method differs from this approach in that we use a continuous time trajectory representation [5], maximizing the measure using batch optimization. To our knowledge this is the first time that a continuous trajectory representation and batch optimization method have been used for singularity avoidance.

Multiple state of the art motion planning algorithms [1], [2], [12], [13] attempt to find a sequence of states and controls which minimize a given objective function while satisfying task constraints. Our method falls into the *trajectory optimization* category, where an initial trajectory is modified using optimization methods. The approach introduced in [6], [7], and used in our work, formulates the motion planning problem as probabilistic inference on a factor graph, finding a maximum likelihood estimate while satisfying constraints given in the form of conditional probabilities. By viewing the problem in this manner, singularities are avoided during planning and replanning by leveraging tools developed for Simultaneous Localization and Mapping (SLAM) purposes such as incremental Smoothing and Mapping (iSAM2) [14]. Adaptation to goal, state, and environment changes is accomplished by re-running the planning algorithm with the previously calculated trajectory as a prior.

III. SINGULARITIES

Consider a joint configuration θ_i as the state of a trajectory θ at time τ_i . The kinematic relationship between configuration and task space velocities at θ_i for an n -DOF robot is defined as

$$\dot{\mathbf{x}} = \mathbf{J}\boldsymbol{\omega}, \quad (1)$$

where $\mathbf{J} \in \mathbb{R}^{m \times n}$ is the robot Jacobian matrix at θ_i , while $\boldsymbol{\omega} \in \mathbb{R}^n$ and $\dot{\mathbf{x}} \in \mathbb{R}^m$ are the configuration and task space velocities at τ_i , respectively. Considering an n -dimensional ellipsoid in the space of unit configuration velocities $\|\boldsymbol{\omega}\|^2 = 1$, we can define the mapping to the task space as

$$\|\boldsymbol{\omega}\|^2 = \dot{\mathbf{x}}^T (\mathbf{J}\mathbf{J}^T)^{-1} \dot{\mathbf{x}}. \quad (2)$$

From Eq. (2) we see that scaling of configuration velocities to the task space depends on the conditioning of the positive-definite matrix $\mathbf{J}\mathbf{J}^T$. Configurations resulting in the matrix $\mathbf{J}\mathbf{J}^T$ being non-invertible are termed *singularities*.

A. Manipulability

This section introduces the manipulability measure used to define a likelihood associated with singularity avoidance. As we only test our method on kinematic chains within a Cartesian task space, we restrict our analysis to this class of problems. However, the notion of a singularity is generalizable to any type of task and robotic system.

Manipulability is the capacity for a change in pose of a robot frame given a configuration [4]. It is associated with the ellipsoid defined by Eq. (2), which in Euclidean space is known as the *manipulability ellipsoid* [15]. The principal axes $\sigma_1 \mathbf{u}_1, \sigma_2 \mathbf{u}_2, \dots, \sigma_m \mathbf{u}_m$ of this ellipsoid can be determined through singular value decomposition $\mathbf{J} = \mathbf{U}\boldsymbol{\Sigma}\mathbf{V}^T$. The manipulability measure of a kinematic chain at θ_i is then proportional to the volume \mathcal{V} [15] of the manipulability ellipsoid

$$\lambda = \sqrt{\det(\mathbf{J}\mathbf{J}^T)} = \sqrt{\sigma_1 \sigma_2 \dots \sigma_m}. \quad (3)$$

The value $\sigma_k \geq 0$ is the k -th largest singular value of $\mathbf{J}\mathbf{J}^T$. A low manipulability value corresponds to a low volume of the manipulability ellipsoid, inhibiting motion in the task space. An example of the manipulability ellipsoid of the end effector frame of a simple manipulator is depicted in Fig. 2.

Unfortunately, manipulability is a non-convex function and using it in any optimization procedure requires convexification. The gradient can be calculated numerically, but it is also possible to derive its change with respect to the j -th joint of the configuration θ_i using Jacobi's identity:

$$\frac{\partial \lambda}{\partial \theta_{i,j}} = \frac{\lambda}{2} \text{Tr} \left((\mathbf{J}\mathbf{J}^T)^{-1} \left(\frac{\partial \mathbf{J}}{\partial \theta_{i,j}} \mathbf{J}^T + \mathbf{J} \frac{\partial \mathbf{J}^T}{\partial \theta_{i,j}} \right) \right). \quad (4)$$

While the inversion $(\mathbf{J}\mathbf{J}^T)^{-1}$ is generally computationally expensive to calculate, in a motion planning context these values are also used to maintain kinematic constraints. Further, the gradient $\frac{\partial \mathbf{J}}{\partial \theta_{i,j}}$ is a component of the robot Hessian matrix and can be constructed using elements of the Jacobian [16].

B. Singularity avoidance likelihood

Consider a kinematic chain and corresponding manipulability ellipsoid with a volume $\mathcal{V}(\theta_i)$, as shown in Fig. 2. We define a minimum acceptable ellipsoid volume $\mathcal{V}_S > 0$, assuming that it implies at least one singular value is near zero. We regard configurations resulting in a manipulability $\lambda(\mathcal{V}(\theta_S)) < \lambda(\mathcal{V}_S)$ to be *near singular*.

Conversely, a high manipulability value does not imply that a configuration is not nearly singular, as an ellipsoid with one 'degenerate' (i.e., of very small magnitude) axis can still have a large volume. However, assuming the volume of manipulability ellipsoids for the chain is bounded by the value $\mathcal{V}_{max} < \infty$ with the axes $\sigma_1 \|\mathbf{u}_1\|, \sigma_2 \|\mathbf{u}_2\|, \dots, \sigma_m \|\mathbf{u}_m\| \geq \epsilon >$

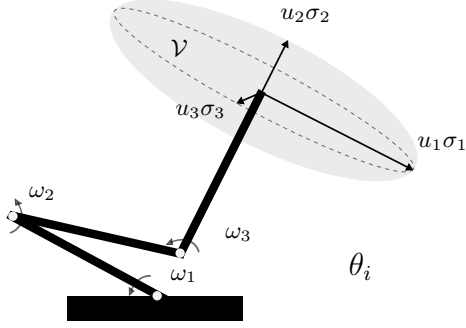


Fig. 2: Illustration of the manipulability ellipsoid of volume \mathcal{V} for a manipulator end-effector at configuration θ_i . Larger axis lengths indicates higher mobility.

0 being of an acceptable length for all such ellipsoids, we infer that configurations whose ellipsoid volume is sufficiently close to \mathcal{V}_{max} are not nearly singular.

An intuitive way to reason about nearly singular configurations via probabilistic inference is by defining the likelihood of a given configuration not being nearly singular as:

$$L(\theta_i|\bar{S}) \propto p(\bar{S}|\theta_i). \quad (5)$$

By modelling the distribution in Eq. (5), we can optimize a trajectory prior to avoid singularities by maximizing the corresponding likelihood. The algorithm described in Section IV requires the distribution of (5) to take the form

$$p(\bar{S}|\theta_i) = \exp\left\{-\frac{1}{2}\|h_{\bar{S},i}\|_{\Sigma_{\bar{S}}}^2\right\}. \quad (6)$$

As the manipulability measure is proportional to a m -dimensional volume, its value can vary by several orders of magnitude throughout a given trajectory. In order to compensate for this volatility, we choose the cost $h_{\bar{S},i}$ to be logarithmic¹,

$$h_{\bar{S},i} = \ln\left(\frac{\lambda_{max}}{\lambda}\right), \quad (7)$$

where the value λ_{max} is the manipulability value at \mathcal{V}_{max} . This makes the cost gradient,

$$\frac{\partial h_{\bar{S},i}}{\partial \theta_{i,j}} = -\frac{\lambda_{max}}{2} Tr\left(\left(\mathbf{J}\mathbf{J}^T\right)^{-1}\left(\frac{\partial \mathbf{J}}{\partial \theta_{i,j}}\mathbf{J}^T + \mathbf{J}\frac{\partial \mathbf{J}}{\partial \theta_{i,j}}^T\right)\right), \quad (8)$$

scale well by canceling out the λ occurring in Eq. (4).

Assuming an exponential distribution for the trajectory prior $p(\theta)$, finding a trajectory maximizing the likelihood in Eq. (6) takes the form of a MAP problem.

IV. TRAJECTORY OPTIMIZATION AS PROBABILISTIC INFERENCE

This section describes the trajectory optimization framework used to maximize the singularity avoidance likelihood

¹Viewing $\Sigma_{\bar{S}}$ as a covariance matrix implies that $\frac{1}{\lambda}$ has a log-normal probability density function.

defined by Eq. (7). The continuous time Gaussian process trajectory representation, first used in [5] in the context of estimation, is described in Section IV-A. Section IV-B shows how optimizing a trajectory represented in such a manner can be performed as inference on a factor graph, as is done in [6], [7], [17].

A. Gaussian processes as trajectory representations

A continuous-time trajectory is considered as a sample from a vector-valued Gaussian process (GP), $\theta(t) \sim \mathcal{GP}(\mu(t), \mathbf{K}(t, t'))$, with mean $\mu(t)$ and covariance $\mathbf{K}(t, t')$, generated by a linear time-varying stochastic differential equation (LTV-SDE)

$$\dot{\theta}(t) = \mathbf{A}(t)\theta(t) + \mathbf{u}(t) + \mathbf{F}(t)\mathbf{w}(t), \quad (9)$$

where \mathbf{A} , \mathbf{F} are system matrices, \mathbf{u} is a known control input and $\mathbf{w}(t)$ is generated by a white noise process. The white noise process is itself a GP with zero mean value

$$\mathbf{w}(t) \sim \mathcal{GP}(\mathbf{0}, \mathbf{Q}_c\delta(t-t')), \quad (10)$$

where \mathbf{Q}_c is a power spectral density matrix.

The solution of the LTV-SDE in Eq. (9) is generated by the mean and power spectral density of the GP:

$$\mu(t) = \Phi(t, t_0)\mu_0 + \int_{t_0}^t \Phi(t, s)\mathbf{u}(s)ds \quad (11)$$

$$\mathbf{K}(t, t') = \Phi(t, t_0)\mathbf{K}_0\Phi(t', t_0)^T + \int_{t_0}^{\min(t, t')} \Phi(t, s)\mathbf{F}(s)\mathbf{Q}_c\mathbf{F}(s)^T\Phi(t', s)ds, \quad (12)$$

where μ_0 , \mathbf{K}_0 are initial mean and covariance of the first state, and $\Phi(t, s)$ is the state transition matrix [5].

The GP prior distribution is then given in terms of its mean μ and covariance \mathbf{K} :

$$p(\theta) \propto \exp\left\{-\frac{1}{2}\|\theta - \mu\|_{\mathbf{K}}^2\right\}. \quad (13)$$

Due to the Markov property of the LTV-SDE in Eq. (9), the inverse kernel matrix \mathbf{K}^{-1} of this prior is exactly sparse block tridiagonal [5]

$$\mathbf{K}^{-1} = \mathbf{A}^{-T}\mathbf{Q}^{-1}\mathbf{A}^{-1}, \quad (14)$$

where

$$\mathbf{A}^{-1} = \begin{bmatrix} \mathbf{1} & 0 & \dots & 0 & 0 \\ -\Phi(t_1, t_0) & \mathbf{1} & \dots & 0 & 0 \\ 0 & -\Phi(t_2, t_1) & \ddots & \vdots & \vdots \\ \vdots & \vdots & \ddots & \mathbf{1} & 0 \\ 0 & 0 & \dots & -\Phi(t_N, t_{N-1}) & \mathbf{1} \end{bmatrix} \quad (15)$$

and

$$\mathbf{Q}^{-1} = \text{diag}(\mathbf{K}_0^{-1}, \mathbf{Q}_{0,1}^{-1}, \dots, \mathbf{Q}_{N-1,N}^{-1}) \quad (16)$$

with

$$\mathbf{Q}_{a,b} = \int_{t_a}^{t_b} \Phi(b, s)\mathbf{F}(s)\mathbf{Q}_c\mathbf{F}(s)^T\Phi(b, s)ds, \quad (17)$$

for the trajectory going from t_0 to t_N , and \mathbf{K}_0 being the initial covariance. As it will be shown in Section IV-B, this kernel allows for fast, structure-exploiting inference and is the key benefit of the prior proposed in Eq. (13).

Another major benefit of using Gaussian processes to model continuous-time trajectories in motion planning is the possibility to query the planned state $\boldsymbol{\theta}(\tau)$ at any time of interest τ , and not only at discrete time instants. If the prior proposed in Eq. (13) is used, GP interpolation can be performed efficiently due to the aforementioned Markovian property of the LTV-SDE in Eq. (9). State $\boldsymbol{\theta}(\tau)$ at $\tau \in [t_i, t_{i+1}]$ is a function of only its neighboring states [7],

$$\boldsymbol{\theta}(\tau) = \boldsymbol{\mu}(\tau) + \boldsymbol{\Lambda}(\tau)(\boldsymbol{\theta}_i - \boldsymbol{\mu}_i) + \boldsymbol{\Psi}(\tau)(\boldsymbol{\theta}_{i+1} - \boldsymbol{\mu}_{i+1}), \quad (18)$$

$$\boldsymbol{\Lambda}(\tau) = \boldsymbol{\Phi}(\tau, t_i) - \boldsymbol{\Psi}(\tau)\boldsymbol{\Phi}(t_{i+1}, t_i), \quad (19)$$

$$\boldsymbol{\Psi}(\tau) = \mathbf{Q}_{i,\tau}\boldsymbol{\Phi}(t_{i+1}, \tau)^T\mathbf{Q}_{i,i+1}^{-1}, \quad (20)$$

where $\mathbf{Q}_{a,b}$ is given in Eq. (17). The fact that any state $\boldsymbol{\theta}(\tau)$ can be computed in $O(1)$ can be exploited for efficient computation of obstacle and singularity avoidance costs.

B. Trajectory optimization as probabilistic inference

To formulate the trajectory optimization problem as probabilistic inference, we seek to find a trajectory parametrized by $\boldsymbol{\theta}$ given desired events e . The posterior density of $\boldsymbol{\theta}$ given events e can be computed via Bayes' rule from a prior and likelihood

$$p(\boldsymbol{\theta} | e) = p(\boldsymbol{\theta})p(e | \boldsymbol{\theta})/p(e) \propto p(\boldsymbol{\theta})p(e | \boldsymbol{\theta}), \quad (21)$$

where $p(\boldsymbol{\theta})$ represents the prior on $\boldsymbol{\theta}$ which encourages smoothness of the trajectory, while $p(e | \boldsymbol{\theta})$ represents the probability of the desired events occurring given $\boldsymbol{\theta}$. The optimal trajectory $\boldsymbol{\theta}$ is found by maximizing the posterior $p(\boldsymbol{\theta} | e)$, using the *maximum a posteriori* (MAP) estimator

$$\boldsymbol{\theta}^* = \arg \max_{\boldsymbol{\theta}} p(\boldsymbol{\theta}) p(e | \boldsymbol{\theta}), \quad (22)$$

where

$$p(e | \boldsymbol{\theta}) = \prod_i p(e | \boldsymbol{\theta}_i) \quad (23)$$

with $\boldsymbol{\theta}_i$ being the configuration at discrete time instant t_i . Given that the desired events for a configuration $\boldsymbol{\theta}_i$ are independent, the probability $p(e | \boldsymbol{\theta}_i)$ can be factored into the product of individual terms

$$p(e | \boldsymbol{\theta}_i) = \prod_k p(e_k | \boldsymbol{\theta}_i). \quad (24)$$

The individual terms are conditional distributions which, given the configuration $\boldsymbol{\theta}_i$, specify the likelihood of the events occurring

$$L_k(\boldsymbol{\theta}_i | e_k) \propto p(e_k | \boldsymbol{\theta}_i). \quad (25)$$

The likelihoods are defined as distributions in the exponential family

$$L_k(\boldsymbol{\theta}_i | e_k) \propto \exp\left\{-\frac{1}{2}\|\mathbf{h}_k(\boldsymbol{\theta}_i)\|_{\boldsymbol{\Sigma}_k}^2\right\}, \quad (26)$$

where $\mathbf{h}_k(\boldsymbol{\theta}_i)$ is an arbitrary function that is used to incorporate desired constraints into the MAP formulation.

Deriving the MAP trajectory from Eq. (22) in a similar manner to [7], our *maximum a posteriori* trajectory is

$$\boldsymbol{\theta}^* = \arg \min_{\boldsymbol{\theta}} \left\{ \frac{1}{2}\|\boldsymbol{\theta} - \boldsymbol{\mu}\|_{\mathbf{K}}^2 + \sum_k \frac{1}{2}\|\mathbf{h}_k(\boldsymbol{\theta})\|_{\boldsymbol{\Sigma}_k}^2 \right\}. \quad (27)$$

To obtain the MAP trajectory by solving the aforementioned optimization problem with iterative approaches, such as the Gauss-Newton or Levenberg-Marquardt algorithms, we require a linearized approximation of Eq. (27). Converting the nonlinear least squares problem to a linear problem around the operating point $\bar{\boldsymbol{\theta}}$, the following expression for the optimal perturbation $\delta\boldsymbol{\theta}^*$ is obtained,

$$\delta\boldsymbol{\theta}^* = \arg \min_{\delta\boldsymbol{\theta}} \left\{ \frac{1}{2}\|\bar{\boldsymbol{\theta}} + \delta\boldsymbol{\theta} - \boldsymbol{\mu}\|_{\mathbf{K}}^2 + \sum_k \frac{1}{2}\|\mathbf{h}_k(\bar{\boldsymbol{\theta}}) + \mathbf{H}_k\delta\boldsymbol{\theta}\|_{\boldsymbol{\Sigma}_k}^2 \right\}, \quad (28)$$

where

$$\mathbf{H}_k = \text{diag}(\mathbf{H}_{k,0}, \dots, \mathbf{H}_{k,N}), \quad (29)$$

with $\mathbf{H}_{k,i}$ being the Jacobian matrix of $\mathbf{h}_k(\boldsymbol{\theta}_i)$

$$\mathbf{H}_{k,i} = \left. \frac{\partial \mathbf{h}_k(\boldsymbol{\theta}_i)}{\partial \boldsymbol{\theta}_i} \right|_{\bar{\boldsymbol{\theta}}(t_i)} \quad (30)$$

and N the index of the end configuration. The optimal perturbation $\delta\boldsymbol{\theta}^*$ is obtained by solving the following linear system

$$\left(\mathbf{K}^{-1} + \sum_k \mathbf{H}_k^T \boldsymbol{\Sigma}_k^{-1} \mathbf{H}_k \right) \delta\boldsymbol{\theta}^* = \mathbf{K}^{-1}(\boldsymbol{\mu} - \bar{\boldsymbol{\theta}}) - \sum_k \mathbf{H}_k^T \boldsymbol{\Sigma}_k^{-1} \mathbf{h}_k(\bar{\boldsymbol{\theta}}). \quad (31)$$

This MAP trajectory optimization procedure can be represented as inference on a factor graph [18]. The fact that the system in Eq. (31) is linear and sparse can be exploited to find the solution efficiently. In our case, the posterior distribution given by Eq. (21) can be factorized similarly to [19]:

$$P(\boldsymbol{\theta} | e) \propto \prod_{t_i}^N f^{gp}(\boldsymbol{\theta}_i, \boldsymbol{\theta}_{i+1}) f_i^{obs}(\boldsymbol{\theta}_i) f^S(\boldsymbol{\theta}_i) \prod_{\tau=1}^{n_p} f_{i,\tau}^{intp}(\boldsymbol{\theta}_i, \boldsymbol{\theta}_{i+1}), \quad (32)$$

where f^{gp} represents a factor corresponding to a GP prior, f^{obs} represents the collision cost, f^S represents singularity cost and f^{intp} represents the cost calculated for n_p interpolated states that can be obtained by using Eq. (18). Singularity cost factor f^S corresponds to likelihood given in Eq. (5). The factor graph defined in Eq. (32) is depicted in Fig. 3 for a simple trajectory optimization problem with three states.

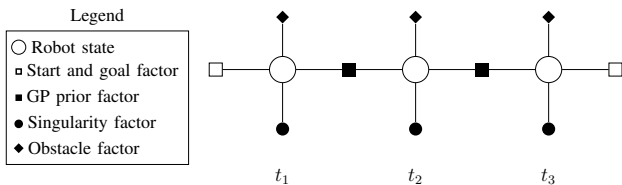


Fig. 3: A simple illustration of the factor graph describing an example trajectory optimization problem with singularity avoidance. GP interpolation factors present between states are omitted for clarity.

V. IMPLEMENTATION DETAILS

We use a GP prior and singularity factors defined in Sections IV-B and III-B, respectively. Additionally we include collision factors used for obstacle avoidance, which we briefly describe in this section. In order for Eq. (24) to hold, we make the assumption that the collision and singularity events are independent,

$$p(e_{obs}, \bar{S} | \theta_i) = p(e_{obs} | \theta_i) p(\bar{S} | \theta_i). \quad (33)$$

A. Cost functions

1) *GP prior*: A double integrator linear system is used for the dynamics of our robot, with white noise injected for the acceleration, meaning that the trajectory is generated by the LTV-SDE in Eq. (9) with

$$\mathbf{A} = \begin{bmatrix} 0 & \mathbf{I} \\ 0 & 0 \end{bmatrix}, \mathbf{u}(t) = 0, \mathbf{F}(t) = \begin{bmatrix} 0 \\ \mathbf{I} \end{bmatrix}. \quad (34)$$

This represents a constant velocity prior which is centred around a zero acceleration trajectory. Applying such a prior will minimize actuator acceleration in the configuration space, thus minimizing the energy consumption, which physically manifests as trajectory “smoothness”. Choosing the GP power spectral density \mathbf{Q}_c has an effect on smoothness, with smaller values penalizing deviation from the prior more.

2) *Collision avoidance*: The collision likelihood is a conditional distribution which, given the current configuration θ_i , specifies the likelihood of being free of collisions

$$L_{obs}(\theta_i | c_i = 0) \propto p_{obs}(c_i = 0 | \theta_i). \quad (35)$$

Similar to the singularity likelihood, the conditional distribution $p_{obs}(c_i = 0 | \theta_i)$ is also formulated to belong to the exponential family and the collision likelihood cost is given as

$$f_i^{obs}(\theta_i) = \exp \left\{ -\frac{1}{2} \| \mathbf{h}_{obs}(\theta_i) \|_{\Sigma_{obs}}^2 \right\}. \quad (36)$$

For collision checking the hinge loss function h_{obs} , a pre-computed signed distance field, is used [6].

3) *Singularity avoidance*: In III-B we choose to represent the likelihood of a given configuration not being in proximity of a singularity as a function of the manipulability measure defined in Eq. (6). We derive the cost

$$f_i^{\bar{S}}(\theta_i) = \exp \left\{ -\frac{1}{2} \| h_{\bar{S},i} \|_{\Sigma_{\bar{S}}}^2 \right\}, \quad (37)$$



Fig. 4: Prior trajectories in Experiment 2, which served as a basis for the random trials.

where $h_{\bar{S}}$ is nonlinear and requires linearization using Eq. (4), resulting in the cost function

$$\tilde{h}_{\bar{S},i} = h_{\bar{S},i} |_{\bar{\theta}_i} + H_{\bar{S},i} |_{\bar{\theta}_i} \delta \theta, \quad (38)$$

with use of the gradient from Eq. (8). The covariance $\Sigma_{\bar{S}}$ is a scalar which “weighs” the costs $h_{\bar{S},i}$ during optimization. Reducing this value causes the optimization to place more weight on singularity avoidance.

B. Measuring improvement

We measure the improvement achieved by our method for an individual trajectory by comparing it to that achieved using the GPMP2 method as described in [7] and summing improvements over individual support and interpolated states

$$M = \sum_{i=0}^N \left(\frac{\lambda}{\lambda_0} - 1 \right). \quad (39)$$

This favours high *relative* improvements at small manipulability values, as the corresponding configurations are more likely to be unacceptably close to singular. In all experiments we optimize over 4 support states, maintaining low problem dimensionality, while using a varying number of interpolated states for additional factors.

C. Software implementation

In our experiments we use the GPMP2 C++ library, and its respective MATLAB toolbox [7], which is based on the GTSAM C++ library [20]. Experiments are performed on a system with a 3.7-GHz Intel Core i7-4800MQ processor and 8 GB of RAM.

VI. RESULTS

We present the results of our method in both a qualitative and quantitative manner. Section VI-A shows qualitatively how our method generates a trajectory that avoids a visibly nearly singular initialization, while respecting obstacle avoidance constraints. In Section VI-B, we choose an inverse kinematics task for three different types of manipulators and run multiple trials, examining the improvement achieved by our method across 200 trajectories.

A. A visibly near-singular trajectory

A nearly singular trajectory similar to the one shown in Fig. 1 is generated by significantly extending the Universal Robots UR-10 arm, a manipulator available in our laboratory, at the elbow joint, losing the capacity to move along its extended axis. We then define an inverse kinematics problem

by taking the end effector position in the final state as a Cartesian goal, while defining the nearly singular trajectory as a prior. The problem is then solved using GPMP2 for two cases, with and without the singularity avoidance factors described in Section III. We choose a singularity avoidance factor covariance value of $\Sigma_{\bar{s}} = 10^{-4}$ with a GP covariance value of $\mathbf{Q}_c = 10^3 \mathbf{I}$. The position goal is defined as a factor on the final state of the factor graph in both cases, while singularity and collision factors are included both at and in-between states, as interpolated factors. We expect our method to increase the manipulability measure over the entire trajectory, escaping the nearly singular prior while maintaining smoothness.

1) *Singularity avoidance:* Fig. 5a shows that our method results in a significant increase in the manipulability measure, as defined by Eq. (39). The standard GPMP2 method results in a smooth solution, and maintains minimum distance from the initial trajectory as governed by the GP prior factors. The change in trajectory achieved by our method is seen in Fig. 5b, demonstrating that the arm is (visibly) less extended and regains its movement capabilities along the previously degenerate axis. The GP prior factors also maintain smoothness in our solution with manipulability optimization, as seen in Fig. 5c, showing that there are no sudden changes in joint values.

2) *Singularity and collision avoidance:* We repeat our test, this time including a table-shaped obstacle placed in the workspace. We choose singularity and collision avoidance factor covariance value of $\Sigma_{\bar{s}} = 10^{-2}$ and $\Sigma_{obs} = 10^{-3} \mathbf{I}$, with a GP power spectral density value of $\mathbf{Q}_c = 10^3 \mathbf{I}$. As the prior is now passing through the table, the collision costs become non-zero. Fig. 6b shows both resulting trajectories as feasible solutions, with our method again achieving a significant improvement in manipulability, which can be seen in Fig. 6a. As shown in Fig. 6c, both trajectories again maintain the smoothness imposed by the prior. This causes the trajectory from the standard GPMP2 method to remain nearly singular, despite avoiding the obstacle. Our method finds a solution with a visibly larger capacity for further motion in the task space, by bending the arm at the elbow to pass directly in front of the table. This is instead of the alternative: following a more conservative trajectory which completely avoids the table but compromises the arms manipulability, with the arm in a near-singular (overextended) configuration throughout the motion

An interesting result can be seen in Fig. 7, which shows how increasing the number of interpolation states affects the manipulability increase. In the first scenario, where no obstacle is present, increasing the number of interpolation states improves the results by a large margin, whereas in the second scenario, with an obstacle, the need to avoid collisions offsets this improvement. A possible explanation is that propagating interpolated gradients for both collision and singularity costs to support states fails to provide clear gradient information for optimizing the support states. Nonetheless, we observe that in all cases, even when avoiding collision, the manipulability values are higher than those in the prior.

B. Random initializations

The second experiment attempts to provide quantitative results that determine how well our method generalizes across different manipulators and tasks. For each manipulator, we defined an inverse kinematics problem as described in Section VI-A, generating a prior by linearly interpolating between start and goal configurations and taking the final end effector position as the goal. We then randomly perturbed each element of the the start and end states in the prior by an amount $\Delta = \mathcal{U}(-k, k)$, re-interpolating afterward to generate a random and less ideal initialization. This serves as a test of robustness, showing how well our algorithm fares for a certain class of task when faced with replanning in response to bad state or goal estimates. We consider trajectories with a final configuration where the distance to the goal is 1 cm or less as ‘successful.’

Table I provides experimental results gathered across trials on three different manipulators over three different values of k . It is evident that the results vary greatly, in accordance with the choice of task and trajectory prior, with the only common trait being positive average and median improvements. We notice that the PR2 arm consistently achieves the lowest improvement, while the UR-10 achieves the highest values even though it posses one less degree of freedom. Significant average and median improvements are recorded in every trial, however, differing only in their magnitude. A visible trend can be seen as k increases, causing lower median and average improvements with higher average, minimum, and maximum solve times. This trend is due to the perturbed trajectory prior resulting in a worse initialization, as well as individual parameters such as desired duration and \mathbf{Q}_c and $\Sigma_{\bar{s}}$ being tuned for a specific task. The method itself can be considered real-time, since even the worst case solving times are on the order of milliseconds.

The high variance in improvement exists due to the fact that the manipulability measure itself is very volatile, with even small changes of the length of one ellipsoid axis (in a high dimensional space) cause large changes in volume. This also causes the high variance in results, since even small movements in the configuration space may significantly affect the manipulability measure.

VII. DISCUSSION

Our method shows a promising new direction for solving singularity avoidance problems, however it still relies upon a large number of hyperparameters, such as the individual factor covariances. When tuned for a specific task, the interplay of our method with collision avoidance methods provides an interesting advantage over other common approaches.

While improvement is possible with the use of interpolated factors, we note that using them in combination with interpolated obstacle avoidance factors usually resulted in lower manipulability values than when not using them. Nonetheless, the values were still higher than in the unoptimized case.

Deeper insights into the definition of the singularity likelihood could result in an interesting extension to our method,

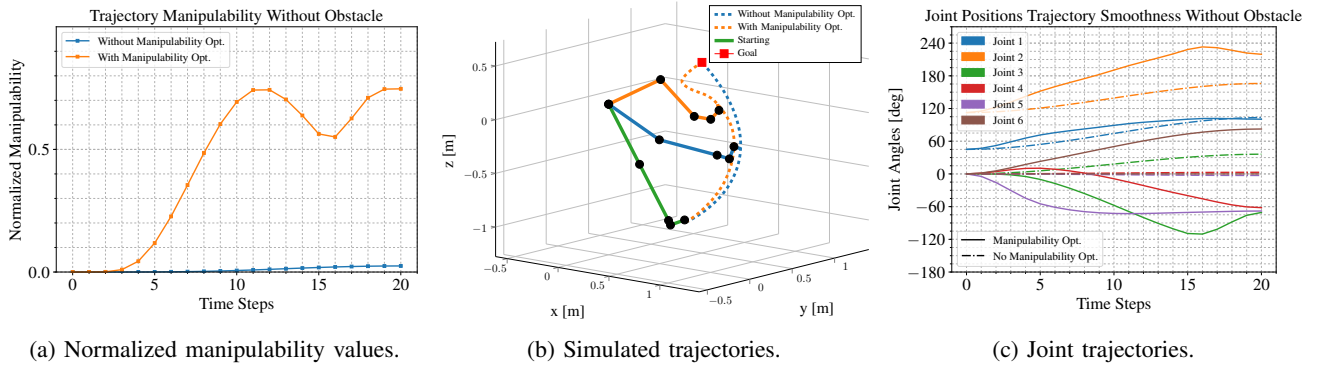


Fig. 5: Experiment 1 results for both the prior and optimized trajectory, without collision avoidance. The values are normalized to the maximum observed manipulability value of 2.93.

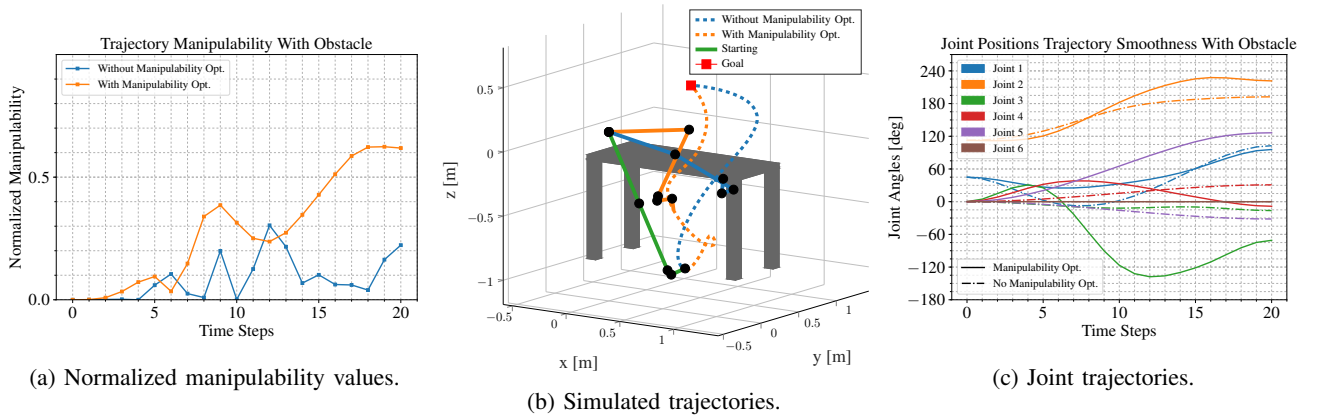


Fig. 6: Experiment one results for both the prior and optimized trajectory with collision avoidance included. The values are normalized to the maximum observed manipulability value of 2.93.

TABLE I: Results per trial for three levels of prior perturbation.

k (Rad)	Manipulator	Improvement		Manipulability		Task	Solving time		
		Median (%)	Avg. (%)	Avg. Initial	Avg. Final	Success (%)	Avg. (ms)	Min (ms)	Max (ms)
$\frac{\pi}{36}$	UR-10	281.65	653.20	0.0086	0.2332	99.50	5.3688	2.4610	16.153
	WAM	17.44	50.99	0.0100	0.1413	94.50	5.3973	2.5350	15.050
	PR2	3.22	9.67	0.0044	0.0855	97.00	5.1463	2.8610	9.1750
$\frac{\pi}{18}$	UR-10	338.24	937.77	0.0162	0.2247	98.00	7.1936	2.5420	14.779
	WAM	19.29	95.32	0.0099	0.1418	90.00	5.9112	2.5510	18.153
	PR2	2.65	16.50	0.0081	0.0866	87.50	5.4891	3.3500	8.8740
$\frac{\pi}{6}$	UR-10	65.96	403.39	0.0367	0.1734	95.50	8.6157	2.4700	19.740
	WAM	8.64	143.25	0.0157	0.1417	83.50	7.0202	3.3500	24.360
	PR2	3.18	14.22	0.0020	0.0853	94.50	5.8490	2.8200	11.843

as we do not provide a formal treatment of the idea. Furthermore, the method could be improved by having information about the actual manipulability properties of a specific robot, such as the maximum achievable manipulability value. Other metrics for proximity to singularities are available but have yet to be shown to be as useful in optimization.

VIII. CONCLUSION AND FUTURE WORK

In this paper we presented a novel method for avoiding singular configuration during planning and replanning using a continuous time Gaussian trajectory representation. This

allowed us to formulate the problem in a maximum likelihood framework, which for our representation is solvable using a MAP estimator. Preliminary results show significant manipulability improvements, which we presented in our qualitative and quantitative analysis.

Even though preliminary tests demonstrate that our method can be used to achieve rapid replanning with the iSAM2 algorithm, we leave a formal experimental treatment as future work. Examining the performance of this method on more complex systems could provide an insight into its robustness. Lastly, further exploring manipulability ellipsoid

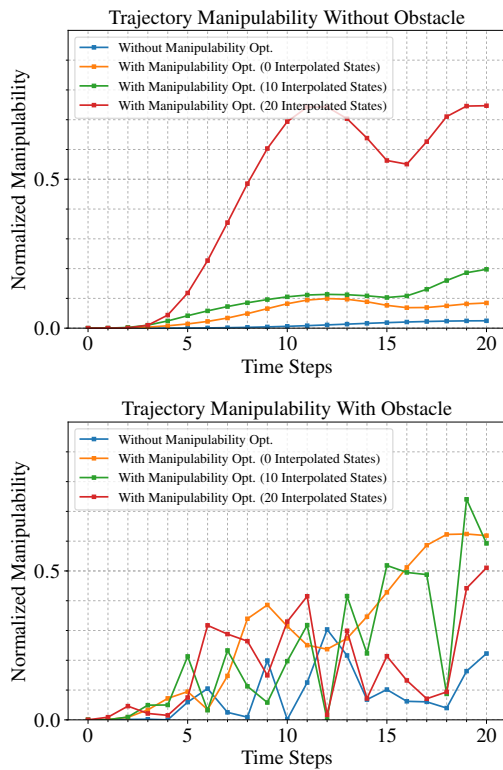


Fig. 7: Increase of manipulability values with a larger number of interpolated states. Values are normalized to the highest observed value.

properties when taking into account configuration uncertainties could prove to be an interesting future research direction.

REFERENCES

[1] N. Ratliff, M. Zucker, J. A. Bagnell, and S. Srinivasa, “CHOMP: Gradient optimization techniques for efficient motion planning,” in *Robotics and Automation, 2009. ICRA’09. IEEE International Conference on*. IEEE, 2009, pp. 489–494.

[2] J. Schulman, J. Ho, A. X. Lee, I. Awwal, H. Bradlow, and P. Abbeel, “Finding Locally Optimal, Collision-Free Trajectories with Sequential Convex Optimization.” in *Robotics: science and systems*, vol. 9, no. 1, 2013, pp. 1–10.

[3] S. Moe, G. Antonelli, A. R. Teel, K. Y. Pettersen, and J. Schrimpf, “Set-Based Tasks within the Singularity-Robust Multiple Task-Priority Inverse Kinematics Framework: General Formulation, Stability Anal-

ysis, and Experimental Results,” *Frontiers in Robotics and AI*, vol. 3, p. 16, 2016.

[4] T. Yoshikawa, “Manipulability of robotic mechanisms,” *The international journal of Robotics Research*, vol. 4, no. 2, pp. 3–9, 1985.

[5] T. D. Barfoot, C. H. Tong, and S. Särkkä, “Batch Continuous-Time Trajectory Estimation as Exactly Sparse Gaussian Process Regression,” in *Robotics: Science and Systems*. Citeseer, 2014.

[6] M. Mukadam, J. Dong, X. Yan, F. Dellaert, and B. Boots, “Continuous-time Gaussian process motion planning via probabilistic inference,” *arXiv preprint arXiv:1707.07383*, 2017.

[7] J. Dong, M. Mukadam, F. Dellaert, and B. Boots, “Motion Planning as Probabilistic Inference using Gaussian Processes and Factor Graphs,” in *Proceedings of Robotics: Science and Systems (RSS-2016)*, 2016.

[8] F. Dellaert and M. Kaess, “Square Root SAM: Simultaneous localization and mapping via square root information smoothing,” *The International Journal of Robotics Research*, vol. 25, no. 12, pp. 1181–1203, 2006.

[9] S. Chiaverini, “Singularity-robust task-priority redundancy resolution for real-time kinematic control of robot manipulators,” *IEEE Transactions on Robotics and Automation*, vol. 13, no. 3, pp. 398–410, 1997.

[10] L. Guilamo, J. Kuffner, K. Nishiwaki, and S. Kagami, “Manipulability optimization for trajectory generation,” in *Robotics and Automation, 2006. ICRA 2006. Proceedings 2006 IEEE International Conference on*. IEEE, 2006, pp. 2017–2022.

[11] K. Dufour and W. Suleiman, “On Integrating Manipulability Index into Inverse Kinematics Solver,” in *2017 IEEE/RSJ International Conference on Intelligent Robots and Systems (IROS 2017)*, 2017.

[12] M. Kalakrishnan, S. Chitta, E. Theodorou, P. Pastor, and S. Schaal, “STOMP: Stochastic trajectory optimization for motion planning,” in *Robotics and Automation (ICRA), 2011 IEEE International Conference on*. IEEE, 2011, pp. 4569–4574.

[13] C. Park, J. Pan, and D. Manocha, “ITOMP: Incremental Trajectory Optimization for Real-Time Replanning in Dynamic Environments,” in *ICAPS*, 2012.

[14] M. Kaess, H. Johannsson, R. Roberts, V. Ila, J. J. Leonard, and F. Dellaert, “iSAM2: Incremental smoothing and mapping using the Bayes tree,” *The International Journal of Robotics Research*, vol. 31, no. 2, pp. 216–235, 2012.

[15] L. Sciavicco and B. Siciliano, *Modelling and control of robot manipulators*. Springer Science & Business Media, 2012.

[16] A. Hourtash, “The kinematic hessian and higher derivatives,” in *Computational Intelligence in Robotics and Automation, 2005. CIRA 2005. Proceedings. 2005 IEEE International Symposium on*. IEEE, 2005, pp. 169–174.

[17] J. Dong, B. Boots, and F. Dellaert, “Sparse Gaussian processes for continuous-time trajectory estimation on matrix lie groups,” *arXiv preprint arXiv:1705.06020*, 2017.

[18] F. R. Kschischang, B. J. Frey, and H.-A. Loeliger, “Factor graphs and the sum-product algorithm,” *IEEE Transactions on information theory*, vol. 47, no. 2, pp. 498–519, 2001.

[19] J. Dong, M. Mukadam, F. Dellaert, and B. Boots, “Motion Planning as Probabilistic Inference using Gaussian Processes and Factor Graphs,” in *Robotics: Science and Systems*, vol. 12, 2016.

[20] F. Dellaert, “Factor graphs and GTSAM: A hands-on introduction,” Georgia Institute of Technology, Tech. Rep., 2012.